Journal of Drug Delivery Science and Technology 81 (2023) 104195

Contents lists available at ScienceDirect

Journal of Drug Delivery Science and Technology

journal homepage: www.elsevier.com/locate/jddst

Hyperbranched polymer-based nanoparticle drug delivery platform for the nucleus-targeting in cancer therapy

Ayça Bal-Öztürk [a,b,c,*], Sherif Domingo Tietilu [d], Oğuz Yücel [d], Tuğba Erol [d], Zeynep Püren Akgüner [b], Hakan Darıcı [c,e], Emine Alarcin [f], Serkan Emik [d]

[a] Department of Analytical Chemistry, Faculty of Pharmacy, Istinye University, Istanbul, Turkey
[b] Department of Stem Cell and Tissue Engineering, Institute of Health Sciences, Istinye University, Istanbul, Turkey
[c] 3D Bioprinting Design&Prototyping R&D Center, Istinye University, 34010, Zeytinburnu, Istanbul, Turkey
[d] Department of Chemical Engineering, Faculty of Engineering, Istanbul University-Cerrahpaşa, Avcılar, 34320, Istanbul, Turkey
[e] Department of Histology and Embryology, Faculty of Medicine, Istinye University, Istanbul, Turkey
[f] Department of Pharmaceutical Technology, Faculty of Pharmacy, Marmara University, Istanbul, Turkey

ARTICLE INFO

Keywords:
Folic acid
Targeted drug delivery
Cancer
Hyperbranched polymer
5-Fluorouracil

ABSTRACT

Hyperbranched polymers (HPB) are drawing attention as one of the drug delivery platforms that can encapsulate drugs owing to the internal voids in their three-dimensional construct. It is feasible to develop HBP-based nano-sized drug delivery platforms and improve the efficacy of cancer treatment due to its potential properties. In particular, the contribution of targeted drug delivery systems that can target malignant tissues in the treatment processes is undeniable. For this purpose, modifying an HBP-based nanoparticle delivery system with a targeting molecule is vital. In this study, we synthesized folic acid-modified HBP-based nanoparticles and their physical (DLS, zeta potential) and chemical (FTIR, NMR) characterizations were performed, and finally 5-Fluorouracil (5-FU) was loaded as a model active agent. The release properties (UV-VIS) and release kinetic models of 5-FU-loaded folic acid-modified nanoparticles were investigated in different pHs. *In vitro* cellular activities (MTT, cellular uptake) and targeting properties to the folate receptor (FR) were determined by flow cytometry on HeLa (FR, +) and L929 (FR, -) cells. According to all the results, folic acid-modified HBP-based nanoparticles were efficiently transported to the cell nucleus in the targeted FR + cells, and internalization of nanoparticles in HeLa cells is ~2.5 times higher than L929 cells. All results suggest that folic acid modification to the nanoparticles is critical in folate receptor-positive cancer treatment.

1. Introduction

Despite all technological advances, cancer is one of the leading causes of death. In conventional chemotherapy, which is one of the key approaches used for cancer treatment, antitumor agents can reach tumor tissues (via EPR [1,2]) from the bloodstream, and enter the specific organelles by passing through (depending on concentration gradient) the dense intracellular cytosolic part in the cells [3,4]. Unfortunately, this process is not selective between normal or malignant tissue, and thereby antitumor agents have resulted in serious adverse effects on normal tissues owing to this poor selectivity. Most patients in conventional cancer treatment are negatively affected by systemic toxicity, hair loss, myelosuppression, immune suppression, and inflammation due to the non-selective antitumor agent effects of chemotherapeutic drugs on normal cells [5–9]. Antitumor agents in the bloodstream are rapidly cleared by the reticuloendothelial system (RES) in conventional therapy [10]. The decrease in the antitumor agent due to RES, its effectiveness in the tumor tissue and significantly diminishes the treatment success [10–12]. Nanoscale drug delivery systems (e.g., micelles, dendrimers, polymers, liposomes, gold nanoparticles, iron oxide nanoparticles) provide several advantages like sizes and surface properties, increased solubility of the antitumor agent, prolonged circulation half-life, and improved biodistribution [13]. Thus, considering these advantages and conjugation of these nanoparticle systems with active-targeting moieties are the focus of research to enhance treatment benefit [14–18].

Active-targeting is the addition of a high-affinity ligand to the nanocarrier's surface, and the added ligand selectively binds to the receptor on the target cell. Nanoparticle orientation to the target tissue is

* Corresponding author. Department of Analytical Chemistry, Faculty of Pharmacy, Istinye University, Istanbul, Turkey.
E-mail addresses: aycabal@gmail.com, aozturk@istinye.edu.tr (A. Bal-Öztürk).

https://doi.org/10.1016/j.jddst.2023.104195
Received 8 October 2022; Received in revised form 13 January 2023; Accepted 19 January 2023
Available online 22 January 2023

achieved by the high specificity of the surface-modified ligand (folic acid, biotin, transferrin, EGF, peptides, aptamers) to the target receptor [13,19]. Folic acid (FA), generally used as a targeting agent, is structurally composed of a pteridine ring, glutamic acid and para-aminobenzoate linked by covalent bonds [20]. In active-targeting, FA binds to folate receptor (FR) antibodies, similar to key-lock, and is transferred via receptor-mediated endocytosis to cancer cells that over-expressed FR in various human carcinomas, containing the breast, brain, kidney, and colon [21–23].

Hyperbranched polymers (HBP) are amorphous, highly branched macromolecules with three-dimensional (3D) dendritic structures and are used in several fields such as coatings, biomedicine, energy applications and drug delivery [20,24–26]. HBP's are conveniently prepared and inexpensive, but polydisperse and not symmetrical structures like dendrimers [27]. The structures of HBPs are irregular; the linear, dendritic, and terminal units are randomly distributed, resulting in broad molecular weight distributions. However, it has drawn attention to the design of drug delivery platforms due to internal voids in 3D spherical structures that can be used for the encapsulation of the drugs [28]. HBPs in nanotechnology and drug delivery could contribute to cancer treatments with high drug encapsulation efficiency, and controlled release properties. Besides, targeting molecule modification of HBPs promises a controllable drug delivery system that can be used in cancer treatment directly towards malignant cells.

In this study, multifunctional HBP nanoparticles were developed for use in targeted cancer treatment as an alternative to conventional chemotherapy; their targeting properties and effect on malignant cells have been detailed. For this purpose, firstly an amphiphilic core-shell structure polymer, HBP-MPEG-*b*-PCL, was designed, then after folic acid conjugation was performed to obtain biocompatible and targeted multifunctional polymer. Nanoparticles were fabricated from the synthesized polymer according to the nanoprecipitation method, and all physical and chemical characterizations were carried out. The synthesized nanoparticles were loaded with 5-FU as a model active agent, and their efficacy was investigated in detail HeLa (FR+) and L929 (FR-) cell lines.

2. Experimental

2.1. Materials

All reagents used in the experiments were of analytical reagent grade. 1,6-Hexanediamine, methyl acrylate, 5-Fuorouracil (5-FU), poly (ethylene glycol) methyl ether (MPEG, Mw ~2000 Da), ε-caprolactone (CL), succinic anhydride, Doxorubicin (DOX), folic acid (FA), 4-(*N*,*N*-dimethylamino)pyridine (DMAP), *N*-(3-dimethylaminopropyl)-N′-ethylcarbodiimide hydrochloride (EDAC) and dibutyltin dilaurate, were purchased from Sigma-Aldrich. Ethoxylated trimethylolpropane (Ethoxy-TMP, Mn ~170) was a gift from Perstorp Polyols AB, Sweden. Aluminum chloride was obtained from Merck. Organic solvent includes hexane, dimethyl sulfoxide (DMSO), dichloromethane (DCM), methanol, *N*,*N*-dimethylformamide and (DMF) were purchased from Merck. LysoTracker Green dye (DND-26) was purchased from Life Technologies. Dulbecco's Modified Eagle's Media (DMEM), Roswell Park Memorial Institute (RPMI) 1640 media, Penicillin-Streptomycin (P/S) and Fetal bovine serum (FBS) were purchased from GIBCO.

2.2. Synthesis of hyperbranched polymer

Poly(aminoester)-based HBP was synthesized through the facile two-step process as described in our previous study [29]. In the first step, 2.324 g of 1,6-hexanediamine was dissolved in 10 mL of methanol 135 mL of methyl acrylate was added by stirring, and the reaction was conducted at room temperature (RT) for 52 h. The organic solvent, and residual methyl acrylate were removed by the rotary evaporator. Afterwards, 2 mL of the obtained product and 1 mL of Ethoxy-TMP were poured into a glass-flask equipped with a mechanical stirrer, immersed in a silicone oil bath which was preheated to 120 °C, and then 0.04 g of $AlCl_3$ was added as a catalyst. The reaction was performed at 120 °C for 5 h. Then, the obtained product was dissolved in 15 mL of chloroform, and centrifuged at 7500 rpm, and then filtered using a syringe filter (0.2 μm pore size) to remove $AICI_3$. Afterwards, rotary evaporator was used to evaporate the chloroform. The obtained material, named HBP, was dried at 40 °C under vacuum.

2.3. Synthesis of diblock copolymer (MPEG-b-PCL)

Ring-opening polymerization was used to synthesize MPEG-*b*-PCL diblock polymer as described in our previous study [29]. The reaction was conducted in a glass-flask equipped with a N_2 inlet tube and a mechanical stirrer. 6.07 mL of CL, 5 g of MPEG and dibutyltin dilaurate as catalyst (1% mole of CL) were mixed and stirred at 60 °C for 10 min, and temperature was increased to 120 °C. The reaction was conducted at 120 °C for 24 h. After cooling to RT, DCM was presented to the reaction medium and stirred for 15 min. Subsequently, the obtained material was precipitated with cold methanol, and filtered. The final product, named MPEG-*b*-PCL, was dried at 40 °C under vacuum.

2.4. Synthesis of carboxyl-ended diblock copolymer (MPEG-b-PCL-COOH)

MPEG-*b*-PCL-COOH was prepared as described in our group previously with a minor modification [29]. Firstly, 2 g of MPEG-*b*-PCL diblock polymer was dissolved in 1-4-Dioxane. Then 0.097 g of succinic anhydride and 0.06 g of DMAP were added. The reaction was conducted at RT for 50 h under N_2 atmosphere. Afterwards, the obtained material was precipitated in cold 1:1 (v/v) hexane-diethylether, filtered and dried under vacuum. The obtained carboxyl-terminated MPEG-*b*-PCL diblock polymer was denominated as MPEG-*b*-PCL-COOH.

2.5. Synthesis of HBP-conjugated diblock copolymer (HBP-MPEG-b-PCL)

MPEG-*b*-PCL-COOH was conjugated to the HBP through carbodiimide chemistry between carboxyl units of MPEG-*b*-PCL-COOH and hydroxyl units of HBP chains [30]. Briefly, 1 g of MPEG-*b*-PCL-COOH was dissolved in DMF, and then activated with 50 mg of EDAC for 1 h. Then 100 mg of HBP in 2 ml of DMF solution was added. Afterwards, 30 mg of DMAP was added and reacted for 72 h under N_2 atmosphere at RT. The obtained solution was dialyzed (MWCO:12,000Da) against ultrapure water for 5 days. The final product, named HBP-MPEG-*b*-PCL, was dried by lyophilization.

2.6. Synthesis of folic acid-conjugated diblock copolymer (HBP-MPEG-b-PCL-FA)

The final conjugate, HBP-MPEG-*b*-PCL-FA, was synthesized using carbodiimide chemistry [30]. Briefly, 1 g of HBP-MPEG-*b*-PCL was dissolved in DMSO. Then FA (45 g) was added and mixed for 30 min at RT. Afterwards, 22 mg of EDAC was added, followed by stirring for 1 h to activate carboxyl groups of FA. Subsequently, 13 mg of DMAP was added and the mixture was reacted for 24 h under N_2 atmosphere at RT to allow the FA to conjugate onto the HBP-MPEG-*b*-PCL. Finally, the solution was inserted in a dialysis bag (MWCO 3500Da) and dialyzed against ultrapure water for 5 days. The final product, named HBP-MPEG-*b*-PCL-FA, was dried by lyophilization.

2.7. Preparation of drug-free and drug-loaded nanoparticles

Nanoparticles were obtained by nanoprecipitation (solvent displacement) technique as described in our previous study [29]. In brief, polymer (10 mg) was dissolved in 1 mL of DMF and added dropwise with stirring at 1000 rpm to 9 ml of PBS solution at RT. Stirring was

continued for 3 h at the same speed to form drug-free nanoparticles.

5-FU was completely dissolved in 10 mg/mL polymer solution (polymer dissolved in DMF) with varied concentrations (1/1, 1/0.5, 1/0.25, 1/0.1 and 1/0.05 w/w polymer/drug) and added dropwise with stirring at 1000 rpm to 9 ml of PBS solution at RT, followed by stirring for 3 h to form drug-loaded nanoparticles. The obtained product was dialyzed in a dialysis bag (MWCO 3500 Da) against PBS to eliminate non-entrapped drug. The samples were abbreviated to HBP-MPEG-*b*-PCL-FA-(5-FU). Figure-1 shows the illustration of the blank and 5 FU-loaded nanoparticles.

2.8. In vitro release experiments

In vitro drug release evaluations were assessed by using the dialysis bag technique. Briefly, a certain amount of the lyophilized 5-FU encapsulated samples in 1 mL of pH 5.5 acetate or pH 7.4 PBS buffers placed into a dialysis bag (MWCO: 3500 Da) and then incubated in release medium 20 mL of pH 5.5 acetate or pH 7.4 PBS buffers under the continuous agitation at 37 °C. The 5-FU concentration was assayed by using a UV/VIS spectrophotometer at 270 nm. All release experiments met the sink conditions and were performed in triplicate.

2.9. Characterization

2.9.1. Dynamic light scattering (DLS), Zeta potential and transmission electron microscopy (TEM) analysis

Particle size, polydispersity index (PDI) and zeta potential of the nanoparticles were evaluated by using NanoZS Instrument (Malvern Instruments). Measurements were carried out at 25 °C by injecting 1 ml of suspended nanoparticle solution into the sample chamber of the device. Three consecutive measurements were made for each formulation. The structure of nanoparticles was analyzed using field emission scanning electron microscopy attached with an energy-dispersive X-ray spectroscopy (FEGSEM-EDS; FEI ESEM Quanta 450 FEG).

2.9.2. FTIR and NMR analysis

The structural analysis of the products was elucidated by ATR-FTIR (Fourier Transform Infrared Spectroscopy), ^{1}H NMR (Proton-Nuclear Magnetic Resonance Spectroscopy) and ^{13}C NMR (Carbon-Nuclear Magnetic Resonance Spectroscopy). FTIR spectra were obtained with a Jasco FT/IR-4600 model FTIR device with ATR unit in the range of 4000-500 cm^{-1}. ^{1}H NMR and ^{13}C NMR analyzes were performed with Varian UNITY INOVA instrument (500 MHz).

2.9.3. Measurement of drug loading and encapsulation efficiency

The 5-FU-loaded nanoparticles were weighed and dissolved in ethanol and then centrifuged. Supernatant of the solution was read by UV/VIS spectrophotometer at 270 nm to obtain 5-FU content. The encapsulation efficiency (EE) and drug loading capacity (DLC) of nanoparticles were quantified using the following equations:

$$\%EE = \frac{Drug_{(total)} - Drug_{(free)}}{Drug_{(Total)}} \; x\; 100$$

$$\%DLC = \frac{Drug_{(total)} - Drug_{(free)}}{Nanoparticles_{(mass)}} x\; 100$$

2.10. Cell culture studies

2.10.1. Cell culture

In this study, HeLa and L929 cell lines were selected as model cell lines to investigate the treatment effectiveness of the nanoparticles. Roswell Park Memorial Institute (RPMI) 1640 media and Dulbecco's Modified Eagle's Media (DMEM) supplemented with 10% FBS and 1% P/S were used for the culture of HeLa and L929 cells, respectively.

2.10.2. Cell viability

Cytotoxic effects of drug-free (blank) and drug-loaded nanoparticles on HeLa and L929 cells were evaluated by using MTT test. Firstly, the cells at a density of 5x10^{3} cells/well were seeded in 96-well plates. On the next day, the culture media was replaced by fresh media including nanoparticles at serial concentrations (0.01, 0.25, 0.5, 1, 2 and 5 mg/mL). To perform MTT assay, on the 6, 24, and 48 h of the experiment, the culture medium of each well was discarded and washed with PBS three times to perform MTT assay. Then cell medium (200 μl) and MTT (2 μg/mL and 20 μl) solution were added. After the incubation of the plates at 37 °C for 4 h, the media of each well was gently discarded and DMSO (200 μl) was pipetted into wells for dissolution of the formazan crystals. Subsequently, the plates were incubated at 37 °C for 20 min, and lastly analyzed with a microplate reader (Spektrostar Nano) at 570 nm. Positive and negative controls were cells treated with DMSO and untreated

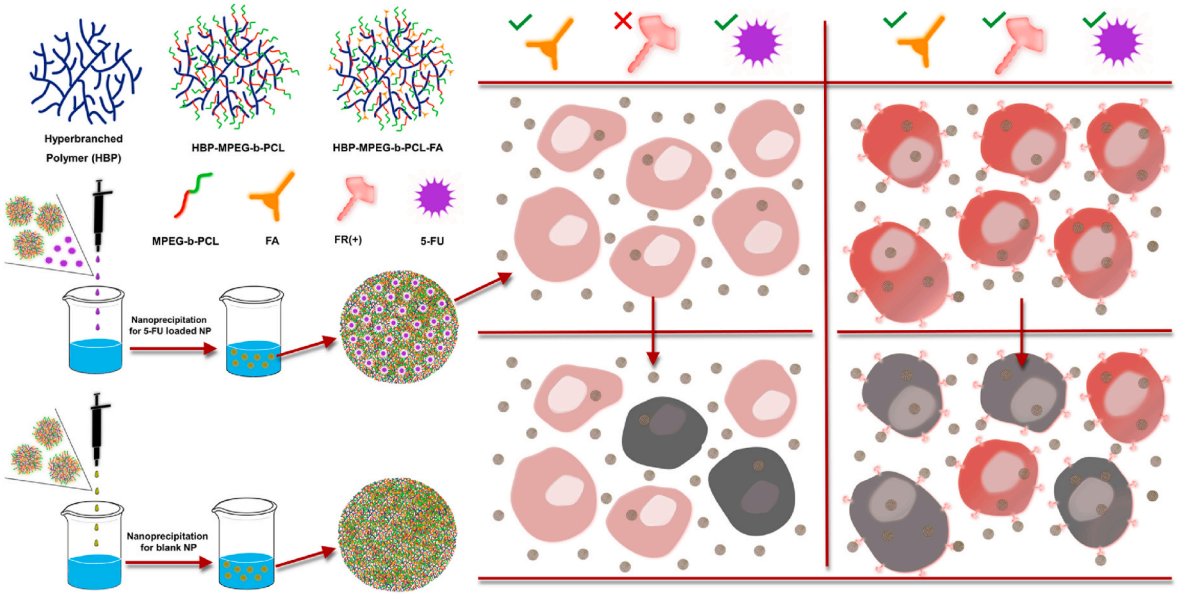

Fig. 1. Illustration of synthesized HBP-MPEG-*b*-PCL-FA structure and nanoparticulation process using with nanoprecipitation method with 5-FU and drug free. HBP-MPEG-*b*-PCL-FA-(5-FU) nanoparticles cytotoxic effect on L929 (FR-) and HeLa (FR+) and schematic representation of notable results of targeted therapy.

cells, respectively. The cytotoxicity of the nanoparticle formulation was quantified by using the following equation:

$$\text{Cell viability } (\%) = \frac{OD570_{(Sample)}}{OD570_{(Control)}} \; x \; 100$$

2.10.3. Cellular uptake

For cellular uptake studies, firstly folic acid modified nanoparticles were labeled with DOX to evaluate the entry of the nanoparticle into the cells. The cells at a density of $2x10^5$ cells/well were seeded in 24-well plates at 37 °C. On the next day, the culture media was replaced by fresh media including nanoparticles. After the incubation at varied time intervals such as 10 min, 30 min, 1 h and 4 h at 37 °C, the culture medium of each well was discarded and washed with PBS three times to remove unbound nanoparticles. Cellular uptake of nanoparticles was followed by the fluorescence property of DOX into HeLa and L929 cells by fluorescence microscope.

2.10.4. Localization analysis

Intracellular localization of nanoparticles in cells was examined by using Lyso tracker and DAPI [31]. Briefly, HeLa cells were seeded at a specific concentration in 24-well plates and incubated for 24 h at 37 °C in 5% CO_2. Then, the media in the wells was discarded and DOX loaded nanoparticle formulations were added. After different incubation times at 37 °C, the wells were washed with PBS three times, fixed with 4% paraformaldehyde, and treated with Lyso Tracker Green (1 μM, 30 min) and DAPI (5 μg/mL, 30 min), respectively. Finally, cells were visualized with a fluorescence microscope (Zeiss, AxioScope Z1).

2.10.5. Flow cytometry

The quantitative evaluations in the cellular uptake studies, flow cytometry was used. Briefly, nanoparticles were treated with HeLa and L929 cells in 24-well plates using the above procedure. After different incubation times at 37 °C, the wells were washed with PBS, harvested with trypsin, and centrifuged to remove the supernatant. Finally, the cells were examined by flow cytometry (BD FACSCALIBUR).

3. Results and discussion

3.1. Chemical characterization of the nanoparticles

In the synthesis of amphiphilic hyperbranched core-shell nanoparticles, the core part is branched poly(amino ester) based polymer (HBP), and the shell part is MPEG-*b*- PCL formed from diblock polymers. Then after with folic acid modification, biocompatible multifunctional polymers (HBP-MPEG-*b*-PCL-FA) were synthesized.

The FTIR spectrum of Monomer 1 given in Figure-2a was interpreted in comparison with the spectra of pure HDA and methyl acrylate. The specific peaks of methyl acrylate were observed 1724 and 1630 cm^{-1} corresponding the carbonyl C═O and vinyl C═C units bands, respectively. The characteristic hexanediamine bands were observed as the asymmetric $–NH_2$ and symmetrical *N*–H bands at 3500 cm^{-1} and 3340 cm^{-1}; the scissoring bands and out-of-plane deformations at 1557 cm^{-1} and 718 cm^{-1}, respectively. In the spectra of Monomer 1, the bands relating to the C═C double bonds and primary amine $–NH_2$ groups were not observed due to the Michael addition among methyl acrylate, and hexanediamine. Additionally, the peak intensity at 1165 cm^{-1} assigned to the C–N bands of the tertiary amine unit increased while the C═O bands due to the methyl acrylate units observed at 1731 cm^{-1} was

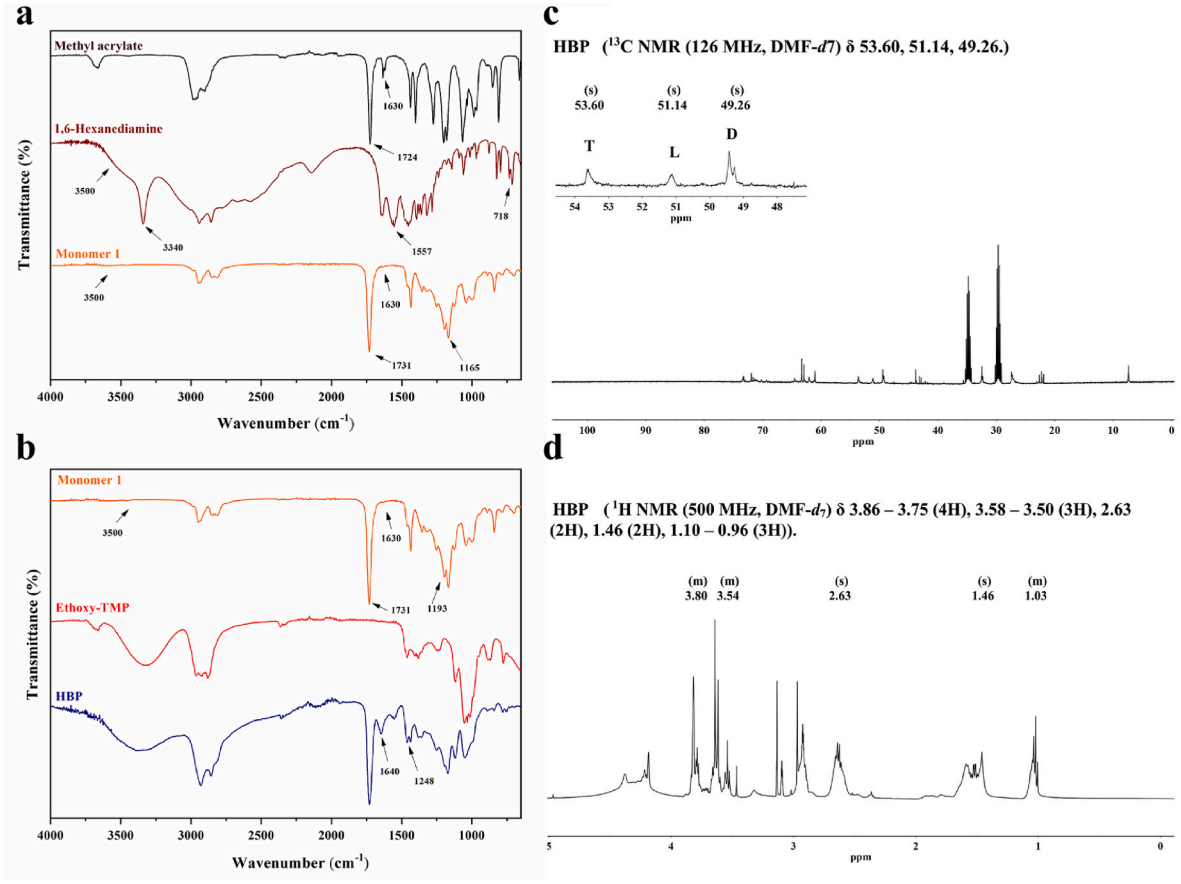

Fig. 2. Characterization of the synthesized polymer by FTIR and NMR: **(a)** FTIR spectra of Monomer 1 synthesis from methyl acrylate and 1,6- hexanediamine, **(b)** FTIR spectra of HBP synthesis from Ethoxy-TMP and Monomer 1, and **(c)** ^{13}C NMR spectrum of HBP, **(d)** ^{1}H NMR spectrum of HBP.

followed. These changes in IR bands depending on the change in the molecular structure indicate that Monomer1 has been successfully synthesized.

Synthesis of HBP was carried out the reaction between Monomer I and Ethoxy-TMP. In the FTIR spectrum of HBP given in Figure-2b the newly formed ester groups as a result of the ester exchange reaction between Monomer I and Ethoxy-TMP, and intermolecular vibrations due to hydrogen bonds are observed at 1640 cm^{-1} [32,33]. Moreover, C–O–C stretching vibrations of methyl ester groups, observed at 1193 cm^{-1} for Monomer I, started to be observed at 1248 cm^{-1} owing to the formation of new ester structures after the ester exchange reaction. HBP structure was illustrated in Figure-1.

The chemical construct of HBP was also confirmed by ^{13}C and ^{1}H NMR analysis (Figure-2c and 2d). The characteristic peaks of HBP in ^{1}H NMR spectra, methyl and methylene protons of the $–CH_2CH_3$ groups in Ethoxy-TMP were determined at 1.03 and 1.46 ppm, respectively. Further, 2.63, 3.54, and 3.80 ppm peaks are the protons in the $–CH_2COO–$, $–COOCH_3$- and $–CH_2CH_2COO–$ groups, respectively. The dendritic (D), linear (L) and terminal (T) signals in ^{13}C NMR spectrum of HBP are recorded at 49.26 ppm, 51.14 ppm, and 53.60 ppm, respectively. In addition, the branching degree (DB) of HBP was calculated by integration of these signals and substituting them in Equation 4. The DB value of the HBP calculated as 0.84, which confirmed that the HBP is branched [34].

$$DB = \frac{D + T}{D + T + L}$$

The FTIR spectra of MPEG-*b*-PCL diblock polymers were given in Figure-3a. The specific IR peaks are ~1722 cm^{-1} ester C═O stretching bands in the PCL and ~1105 cm^{-1} C–O bands in the MPEG, respectively. In ^{1}H NMR analyzes MPEG-*b*-PCL diblock polymer (Figure-3b), the peaks at 3.60 ppm and 3.33 ppm were due to the methylene protons CH_2CH_2O- and -O-CH_3 end units in the PEG blocks, respectively. The peaks of methylene protons of $–(CH_2)_3–$, $–OCCH_2–$ and $–CH_2OOC–$ groups in PCL blocks were determined 1.34, 1.60, 2.26 and 4.01 ppm, respectively. The bands at 4.20 ppm and 3.82 ppm belong to the methylene protons of the -O–CH_2–CH_2- groups in the PEG end blocks associated with the PCL blocks [35]. The NMR and FTIR analysis findings are all in agreement with the literature and confirm a successful synthesis [36].

In order to modify the MPEG-*b*-PCL copolymer to attach to the HBP, MPEG-*b*-PCL was reacted with succinic anhydride for providing to have free carboxyl end units. The FTIR spectrum of obtained product, MPEG-*b*-PCL-COOH, is given in Figure-3a. Besides specific vibrations similar to MPEG-*b*-PCL diblock polymers, prominent C═O vibrations of carboxyl groups were observed in carboxyl modified MPEG-*b*-PCL (MPEG-*b*-PCL-COOH) at 1635 cm^{-1}. Compared with the ^{1}H NMR spectra of MPEG-*b*-PCL-COOH and MPEG-*b*-PCL (Figure-3b), a new peak at around 2.61 ppm was detected. FTIR and NMR results show that carboxyl groups are formed after ring-opening modification with succinic anhydride [37].

HBP-MPEG-*b*-PCL polymers were obtained by the reaction of the hydroxyl end units in the HBP and the carboxyl end groups in the MPEG-*b*-PCL-COOH diblock polymer in the presence of EDAC. In the HBP-MPEG-*b*-PCL spectrum (Figure-4a), both the –OH vibrations of HBP at ~3300-3500 cm^{-1}, and the carboxyl end units peak of the MPEG-*b*-PCL-COOH at about 1635 cm^{-1} were not observed, indicating the successful reaction between these groups.

Finally, The FA conjugation on HBP-MPEG-*b*-PCL were investigated by both FTIR and ^{1}H NMR analysis and the results given in Figure-4b, Figure-4c and Figure-3d. According to the FTIR analyses results, after the modification with FA, the characteristic folic acid C═O stretching vibrations and aromatic ring C═C vibrations were observed in the structure spectra at 1600 cm^{-1} and 1688 cm^{-1}, respectively. In the ^{1}H NMR spectrum given in Figure-4c and Figure-4d compared after folic acid modification, ~8.0 ppm (pteridine group proton 8.23,7.99 and 7.85) peaks were observed, resulting from the aromatic ring of folic acid, consistent with similar studies in the literature [38–47]. These findings confirm that FA molecule was successfully introduced into the HBP structure.

3.2. Size and zeta potentials of the nanoparticles

The nanoparticles prepared from HBP-MPEG-*b*-PCL and HBP-MPEG-*b*-PCL-FA by nanoprecipitation method were further investigated on the basis of particle size, particle size distribution and zeta potential. Accordingly, the particle sizes of HBP-MPEG-*b*-PCL and HBP-MPEG-*b*-PCL-FA nanoparticles were determined as 38.17 ± 3.4, and 41.28 ± 3.7, respectively (Figure-5a and Figure-5b). In addition, the zeta potentials of HBP-MPEG-b-PCL and HBP-MPEG-*b*-PCL-FA structures were determined as −10.2 mV, and −2.26 mV, while the PDI values were almost same and found to be 0.46, and 0.43, respectively. Since the FA contains free amine in its structure; after the modification with FA, the zeta potential of the structure increased, consistent with the literature [48]. The obtained data indicated that the FA modification slightly increased the particle diameter, while significantly increasing the zeta potential, but not intelligibly affecting the particle diameter distribution. The particle size of the 5-FU loaded HBP-MPEG-*b*-PCL-FA nanoparticles was 27.2 nm, the zeta potential was −3.29 mV, and the PDI value was determined 0.636. The DLS result confirmed that with SEM image as given in Figure-5c.

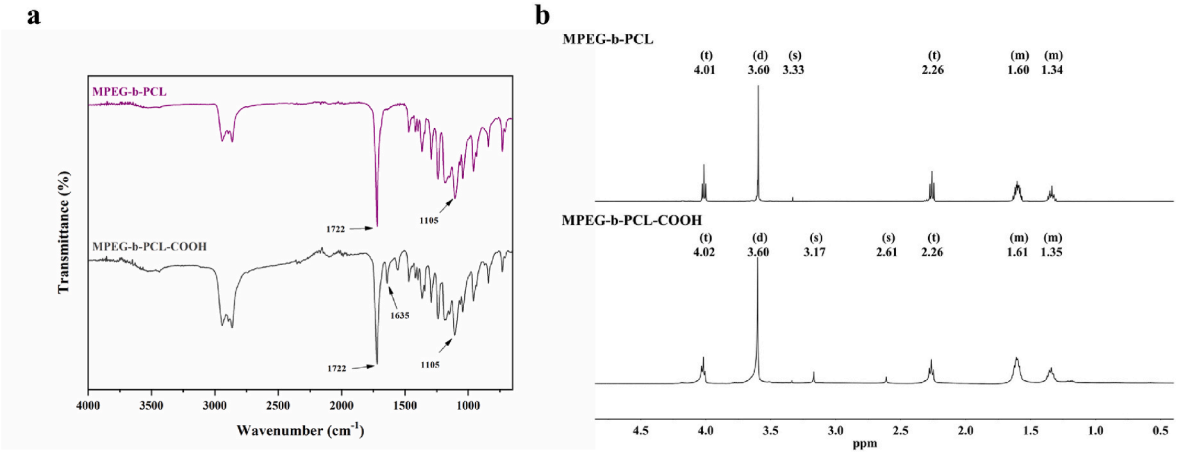

Fig. 3. Characterization of MPEG-*b*-PCL and MPEG-*b*-PCL-COOH by FTIR and NMR: **(a)** FTIR and **(b)** ^{1}H NMR spectra of MPEG-*b*-PCL and MPEG-*b*-PCL-COOH.

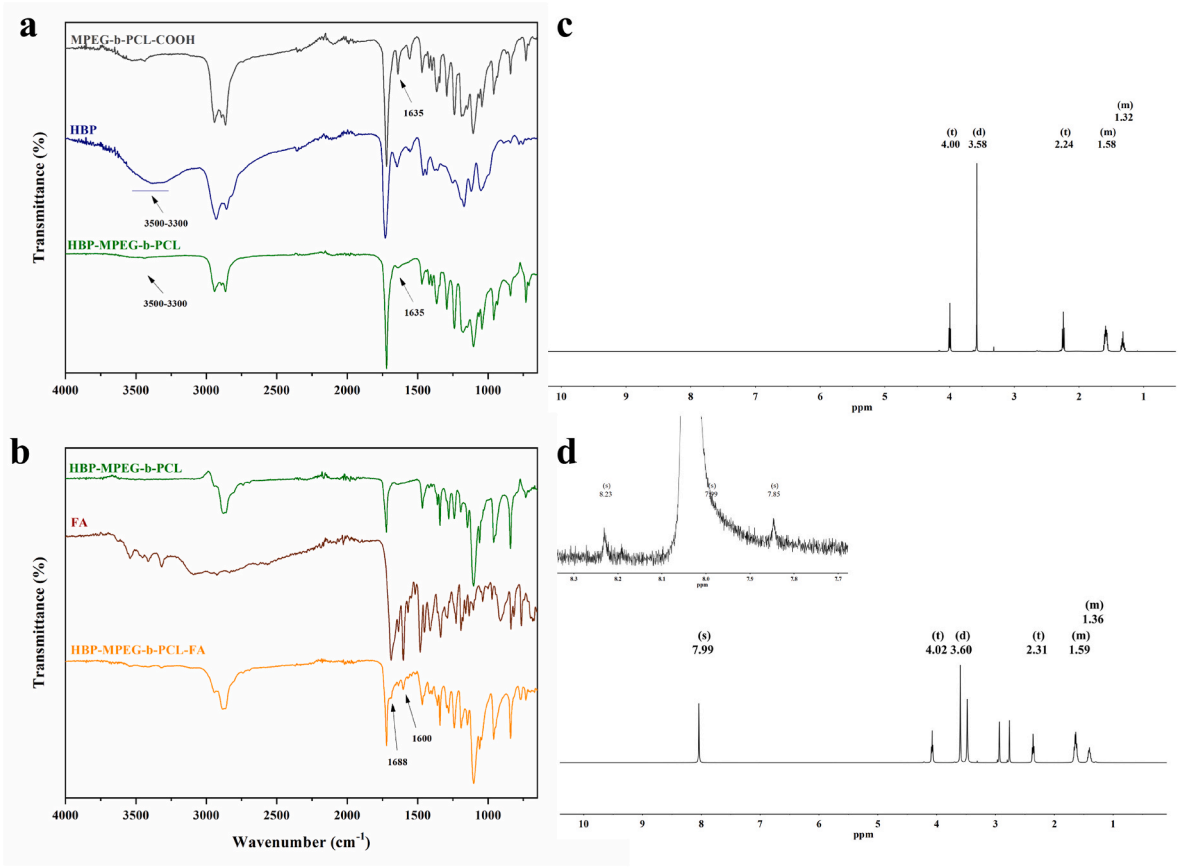

Fig. 4. Chemical structure of HBP-MPEG-*b*-PCL and HBP-MPEG-*b*-PCL-FA characterized by FTIR and NMR: **(a)** FTIR spectra of HBP-MPEG-*b*-PCL synthesis from HBP and MPEG-*b*-PCL, **(b)** FTIR spectra of HBP-MPEG-*b*-PCL-FA synthesis from FA and HBP-MPEG-*b*-PCL, **(c)** ^{1}H NMR spectrum of HBP-MPEG-*b*-PCL and **(d)** ^{1}H NMR spectrum of HBP-MPEG-*b*-PCL-FA.

3.3. Determination of the drug loading and release kinetics of the nanoparticles

An important detail contributing to treatment in nanoparticle systems targeted to cancer cells is that tumors and normal tissues are mostly found at different pHs [49]. In this case, besides the fact that nanoparticle systems allow different amounts of drug release at different pHs, the fact that drug-loaded nanoparticles have minimum drug release (pH 7.4) and sufficient rapid drug release (pH 5.5) in the bloodstream also emerges. An important detail that will contribute to the treatment in nanoparticle systems targeting cancer cells is that tumors and normal tissues, which are located between malignant tissues and intracellular endosomes, are mostly found at different pHs, making significant contributions to the treatment. Drug-loading studies were performed on HBP-MPEG-*b*-PCL-FA nanoparticles and the results were showed in Table-1. According to the results, as the amount of 5-FU increased, the loading capacity percentage of the polymers increased and the loading efficiency percentage decreased [50,51]. This is because the concentration gradient between the aqueous phase and polymer matrix increases, there is much more 5-FU loss in the system and the percent loading efficiency for the nanoparticle decreases [52].

In vitro drug release experiments from nanoparticles were conducted by using the dialysis membrane procedure [53]. In releases, pH 5.5 acetate and pH 7.4 PBS buffer solutions were used as the release media. 5-FU loaded nanoparticles were placed into the dialysis membranes, allowing the drug to pass and release into the medium. Figure-6 shows the cumulative release % of 5-FU from the HBP-MPEG-*b*-PCL-FA nanoparticles loading at 1/0.25 optimum polymer/5-FU (w/w). The release amount was found to be 9% and 2% in the first 6 h at pH 5.5 and pH 7.4, and the end of the 24 h the release at pH 5.5 and pH 7.4 is 34% and 20%, respectively. The cumulative release amount after 7 days was 57% and 40% at pH 5.5 and pH 7.4, respectively. Similarly, the cumulative 5-FU release from the ZWC–PAMAM complex at pH 7.4 was determined as 63% at 38 h [52]. In another study, the release studies performed similar pHs; the release at 120 h was determined 40% and 78% for pH 7.4 and pH 5.5, respectively [54].

Additionally, the compatibility of the release behavior with various release kinetic models was evaluated for the 5-FU release study for two different pHs. Release kinetic models fitted the data using First-Order, Hixson-Crowell and Korsmeyer-Peppas, models and the mathematical expressions of the kinetic models are given in Equation 5-7, respectively. According to the non-linear regression with the models given in Table 2, the highest R_{adj} values were found for the Korsmeyer-Peppas kinetic model, which pointing out the most compatible model for both pHs.

In the Korsmeyer-Peppas kinetic model, n explain the desorption mechanism from the carrier. For spherical platforms, $n < 0.45$ $0.45 < n < 0.85$, $n = 0.85$ and $0.85 < n$ are known as the release mechanisms of Fickian diffusion, non-Fickian diffusion, case II transport and super case II transport, respectively [55,56]. According to Korsmeyer–Peppas model findings, it is showed that 5-FU release was mainly controlled by non-Fickian diffusion in both pH. Non-Fickian drug diffusion refers to drug transport processes in which the relaxation time of the structures forming the nanoparticle and the diffusion time of the solvent progress simultaneously in the solvent medium. The increase in the release amount despite the decreasing pH of the release solution is explained by the effect of the pH-sensitive HBP in the structure. HBPs in nanoparticles are polyaminoester-based materials. The similar studies conducted in the literature [57–59] concluded that the release amount of the entrapped drug increased due to the protonation of the amino groups in the structure in an acidic environment and the repulsive forces between

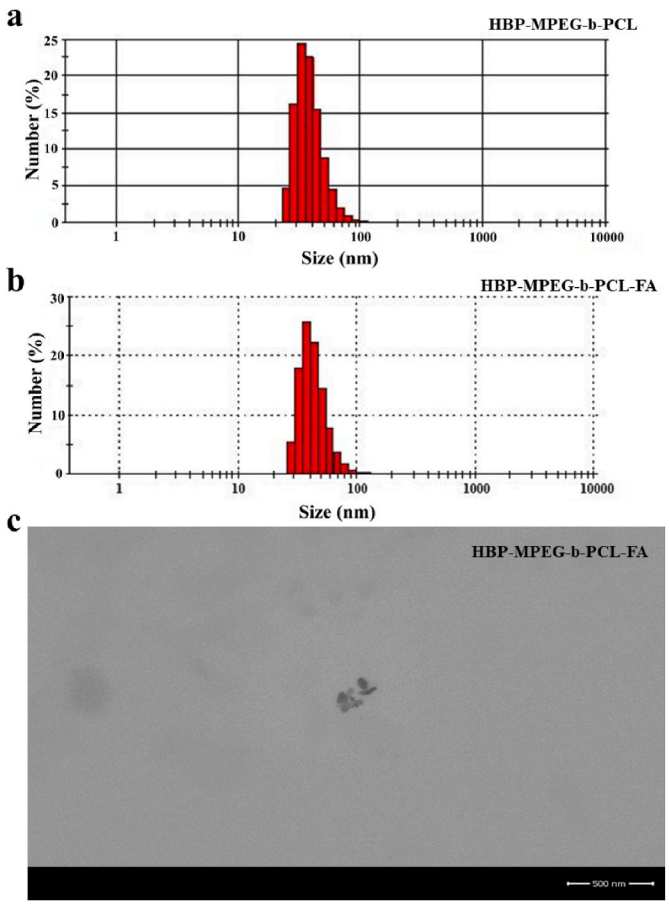

Fig. 5. DLS and TEM measurements of HBP-MPEG-*b*-PCL-FA and HBP-MPEG-*b*-PCL-FA-(5-FU) nanoparticles: **(a)** Size distributions of HBP-MPEG-*b*-PCL-FA measured by DLS, **(b)** Size distributions of HBP-MPEG-*b*-PCL-FA-(5-FU) measured by DLS and **(c)** TEM image of HBP-MPEG-*b*-PCL-FA-(5FU).

Table 1
DLC and EE of HBP-MPEG-b-PCL-FA nanoparticles loaded with 5-FU at different polymer/5-FU ratios.

Polymer/Drug (w/w)	EE (%)	DLC (%)
1/1	19.8	43.0
1/0.5	24.2	28.8
1/0.25	29.9	19.2
1/0.1	37.4	8.7
1/0.05	38.2	5.3

the branches forming the HBP.

$$\ln\left(1-\frac{M_t}{M_\infty}\right) = -K_1 t$$

$$W_0^{\frac{1}{3}} - W_t^{\frac{1}{3}} = K_{HC} t$$

$$\frac{M_t}{M_\infty} = K_{KP} t^n$$

3.4. Cytotoxic effect of 5-FU loaded HBP-PCL-b-MPEG-FA nanoparticles on L929 and HeLa cell lines

In vitro cytotoxic effect of HBP-PCL-*b*-MPEG-FA and 5-FU loaded HBP-PCL-*b*-MPEG-FA nanoparticles was performed by MTT test. It is a colorimetric method based on enzyme activity, generally used to determine the number of viable cells. L929, and HeLa cells were incubated blank, and 5-FU loaded nanoparticles at different concentrations for 6, 24, and 48 h. As shown in Figure-7 and Table S1-S2, the decrease in cell viability of HBP-MPEG-*b*-PCL-FA-(5-FU) nanoparticles increases with incubation time and concentration. In addition, IC_{50} values were calculated according to the literature (Table S3-S4) [60]. IC_{50} values of HBP-MPEG-*b*-PCL-FA nanoparticles against HeLa cells after 6, 24 and 48 h incubation times were found to be 11.41, 4.73 and 3.87 mg/mL, respectively. When the effects of HBP-MPEG-*b*-PCL-FA nanoparticles on L929 and HeLA cells were evaluated together, it was observed that the cell viability decreased from 28.6 ± 3.4% to 5.8 ± 0.9%, respectively, after 48 h of incubation in 5 mg/ml formulations. It has been shown that the toxic effects of the developed particles on HeLA cells are much higher.

When the toxicity results were evaluated together, it was concluded that the HBP-MPEG-*b*-PCL-FA nanoparticles at concentrations of ≤0.5 mg/mL did not have a toxic effect on L929 and HeLa cells. Within the scope of cellular uptake and targeting studies, HBP-MPEG-*b*-PCL-FA nanoparticles at a concentration of 0.5 mg/mL was used. When the results were compared with the literature, the developed HBP-MPEG-*b*-PCL-FA nanoparticles were much less toxic than PAMAM-G6 (IC_{50} = 0.128 mg/mL), gold (IC_{50} = 0.082 mg/mL) and PLGA (IC_{50} = 0.0329 mg/mL) nanoparticles [61–63].

The IC_{50} values of 5-FU loaded HBP-PCL-*b*-MPEG-FA nanoparticles on L929 cells after 6, 24 and 48 h incubation times were found to be 9.28, 3.57 and 1.84 mg/mL, respectively. The IC_{50} values of 5-FU loaded HBP-PCL-*b*-MPEG-FA nanoparticles on HeLa cells after 6, 24 and 48 h incubation times were 7.59, 6.17 and 2.09 mg/mL, respectively. When the cytotoxicity results of pristine nanoparticles and 5Fu loaded nanoparticles were compared, as expected in the literature, 5Fu loaded nanoparticles were more effective against cancer cells. It has been shown to show high toxicity (with lower IC_{50} values) [64–66].

3.5. Cellular uptake and targeting studies for folic acid conjugated nanoparticles on folate receptors

In the targeting study, HeLa (malignant cells, FR +) and L929 (healthy cells FR -) were used to investigate the selective targeting ability of nanoparticles against folate receptors on the cell surface. The clusters in the fluorescent microscope images given in Figure-8 show that the nanoparticles attach to the receptors on the HeLa cell surface and are successfully internalized into the cell via endocytosis. The folic acid unmodified nanoparticles are externalized on the surface of HeLa and L929 cells. It is monitored that HBP-MPEG-*b*-PCL-FA nanoparticles intensely bind to the receptors on the HeLa cell surface within the first 10 min and when the nanoparticles accumulate on the cell surface and were transferred to the HeLa cells via known as endocytosis in time while there is a low non-specific cellular uptake in HBP-MPEG-*b*-PCL nanoparticles without FA. Intracellular localization of nanoparticles in HeLa cells was seen in Figure-9. Results demostrated that the passage of folic acid-modified nanoparticles in and around the cell nucleus within 4 h could be observed over time. These results corresponded well with the observed results in Figure-8.

However, these results do not show a quantitative data for targeting potential of nanoparticles to the cells [67]. In order to observe the targeting properties of nanoparticles from another perspective and to understand receptor specificity and endocytosis, flow cytometry studies were performed with HeLa and L929 cells. As seen in Figure-10, HeLa and L929 cells were used as controls and showed only autofluorescence in both cells as expected. In the flow cytometry results of HBP-MPEG-*b*-PCL-FA nanoparticles incubated with HeLa cells for 10 min to 4 h, the fluorescence intensity increased as the incubation time increased. In contrast, the increased fluorescence intensity of L929 cells was approximately limited. When the results between the two cell lines are evaluated at the end of the 4 h, the number of nanoparticles transferred into the cell in the folate receptor-positive cancer cell line (HeLa) is approximately ~2.5 times higher than in the folate negative cell line

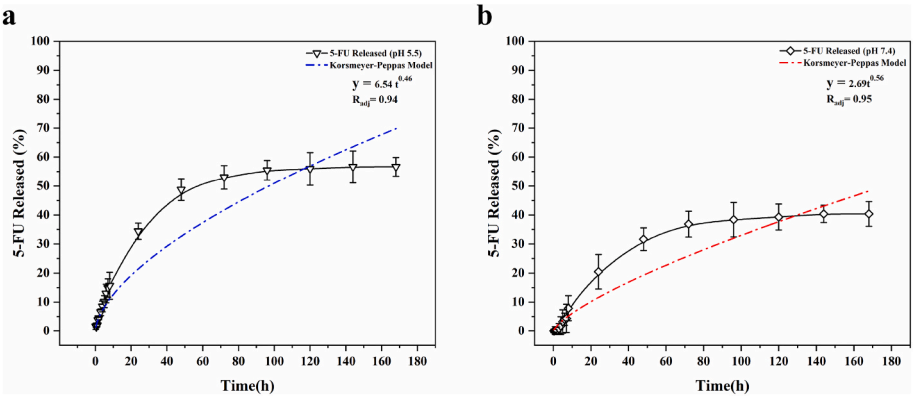

Fig. 6. 5-FU release profiles of HBP-MPEG-*b*-PCL-FA-(5-FU) measurement done by UV-VIS. **(a)** 5-FU cumulative release from HBP-MPEG-*b*-PCL-FA-(5-FU) nanoparticles and fitting release kinetic curve (Korsmeyer-Peppas) in pH 5.5 **(b)** 5-FU cumulative release from HBP-MPEG-*b*-PCL-FA-(5-FU) nanoparticles and fitting release kinetic curve (Korsmeyer-Peppas) in pH 7.4.

Table 2
5-FU released from nanoparticles fitting kinetic models parameters in pH 5.5 and 7.4.

First-Order Kinetic Model	pH **5.5**	**K_1 8.0 x 10^{-3}**	**R_{adj} 0.89**
	pH 7.4	K_1 4.3 × 10^{-3}	R_{adj} 0.85
Hixson-Crowell Kinetic Model	pH 5.5	K_{HC} 2.2 × 10^{-3}	R_{adj} 0.86
	pH 7.4	K_{HC} 1.3 × 10^{-3}	R_{adj} 0.81
Korsmeyer-Peppas Kinetic Model	pH 5.5	n 0.46	R_{adj} 0.94
		K_{KP} 6.54	
	pH 7.4	n 0.56	R_{adj} 0.95
		K_{KP} 2.69	

(L929). All cellular uptake and flow cytometry analysis results determined that folic acid modification of nanoparticles is crucial in folate receptor-positive cancer cell-specific endocytosis.

4. Conclusions

Successful treatment processes can be achieved in cancer treatment day by day. Promising results have been obtained on cell viability and targeting capabilities of HBP-based nanoparticles with their potential use in drug delivery, high drug loading abilities and controlled releases, and active-targeting modification that can accelerate progress in cancer therapy. Studies on cellular uptake and flow cytometry have shown that the synthesized 5-FU loaded-folic acid-modified HBP-based nanoparticle specifically targets folate receptor-positive cancer cells much more than folate negative cancer cells. Nanoparticles have effectively transported up to the cell nucleus in targeted FR + cells. Our study undoubtedly shows that using folic acid-modified HBPs will advance the treatment of folate receptor-positive cancer cells. However, it should be noted that sterilization and depyrogenation processes are of great importance in the evaluation of the safety and efficacy profiles of nanoparticles and therefore in the preclinical development of formulations. It is anticipated that gamma irradiation can be used for both sterilization and depyrogenation of synthesized nanoparticles. Further extensive *in vitro* and *in vivo* studies should be conducted before clinical trials.

Credit author statement

Ayça Bal-Öztürk: Conceptualization, Data curation, Formal analysis, Funding acquisition, Investigation, Methodology, Project

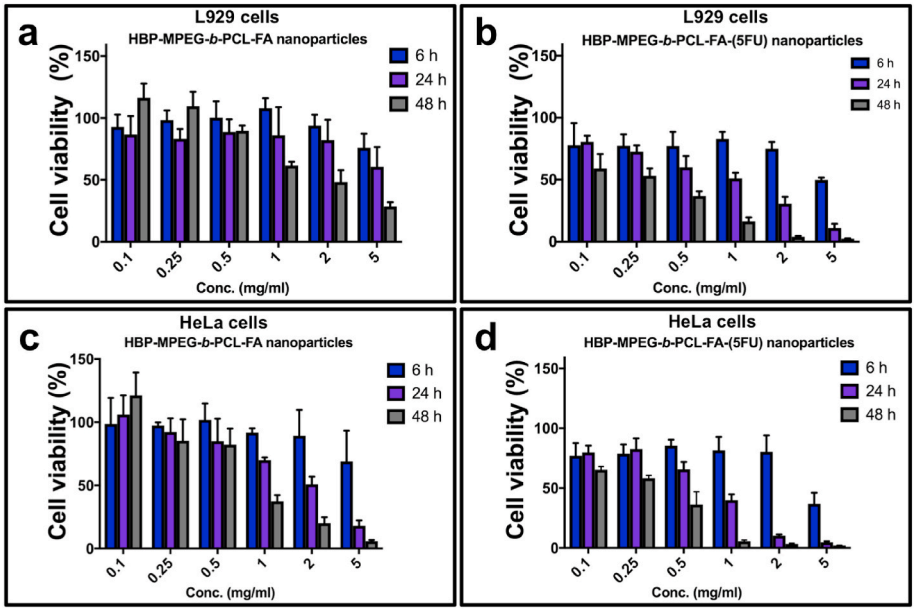

Fig. 7. *In vitro* cytotoxicity of HBP-MPEG-*b*-PCL-FA and HBP-MPEG-*b*-PCL-FA-(5FU) nanoparticles using MTT assay in L929 **(a–b)** and HeLa **(c–d)** cells. The results are given as % cell viability after the incubation with different concentration of nanoparticles for 6 h, 24 h and 48 h. Data are presented as mean ± SD (n = 6).

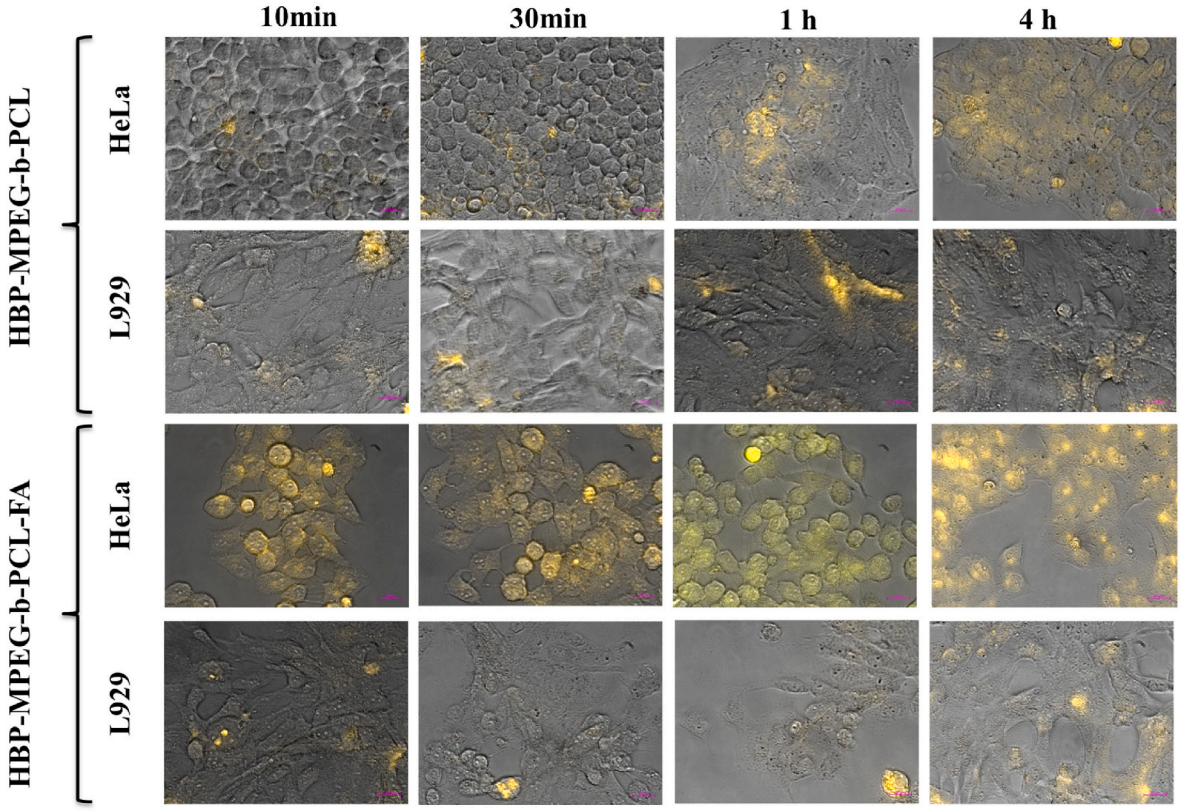

Fig. 8. Qualitative cellular uptake analysis of HBP-MPEG-*b*-PCL and HBP-MPEG-*b*-PCL-FA nanoparticles by HeLa and L929 cells for 10 min, 30 min, 1 h and 4 h. DOX was used to label the nanoparticles. Scale bar: 50 μm.

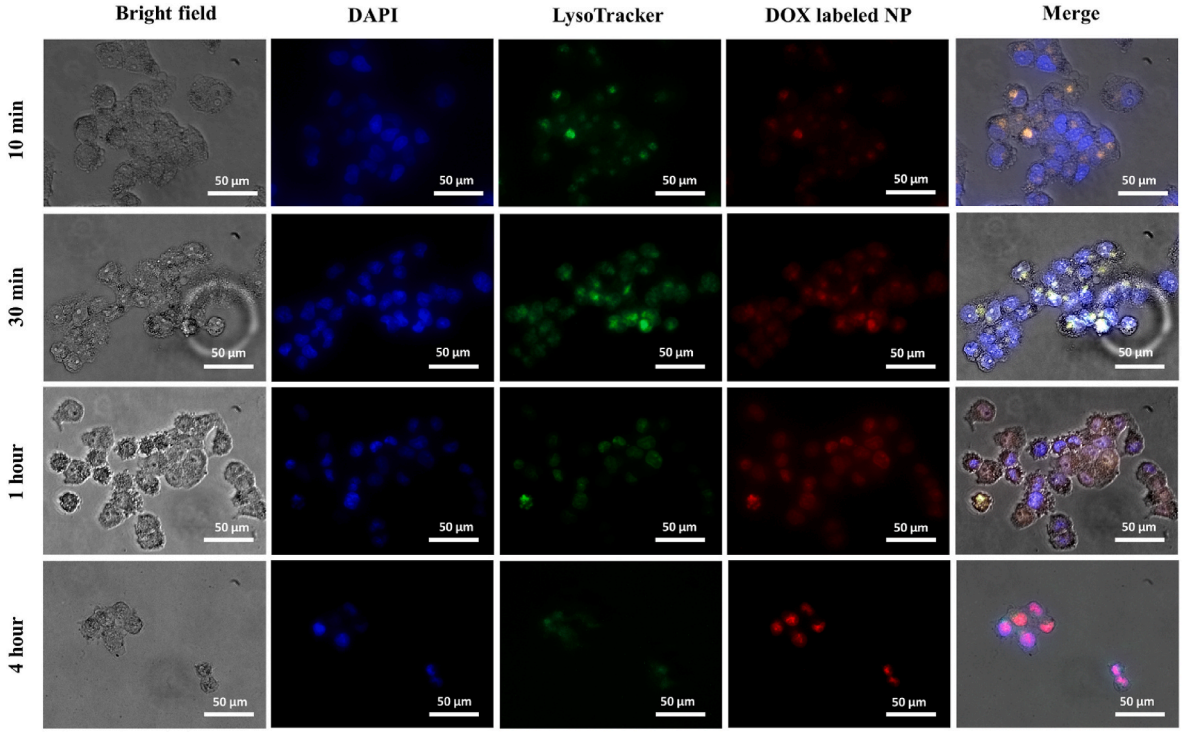

Fig. 9. Fluorescent microscope pictures of HeLa cells after the incubation with HBP-MPEG-*b*-PCL-FA nanoparticles for 10 min, 30 min, 1 h and 4 h. DOX was used to label the nanoparticles. HBP-MPEG-*b*-PCL-FA nanoparticles was successfully internalized by HeLa cells and shows the distribution of nanoparticle inside the cells where blue, green and red colours show fluorescence intensity of DAPI, lysotracker reagent and DOX, respectively. For each panel, pictures from left to right indicate cell morphology, cell nuclei, lysosome and DOX fluorescence (red) and merged pictures. Scale bar: 50 μm. (For interpretation of the references to colour in this figure legend, the reader is referred to the Web version of this article.)

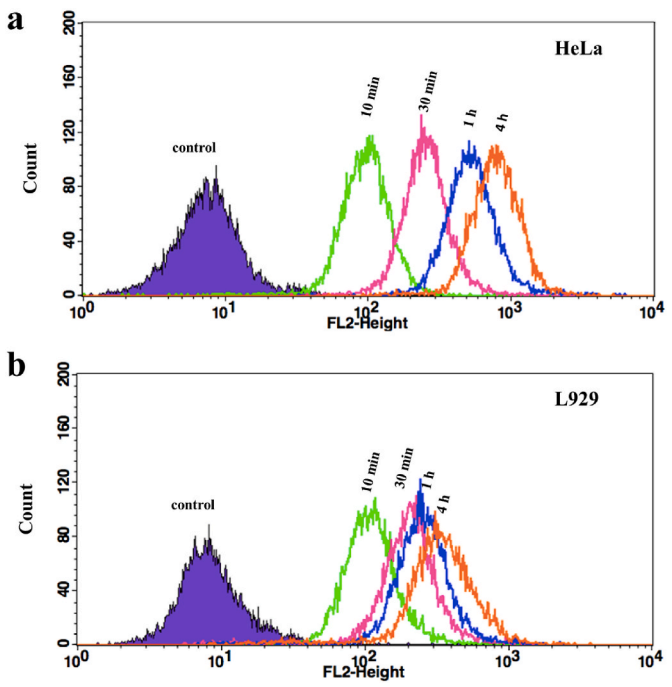

Fig. 10. Flow cytometry portraits of HeLa **(a)** and L929 **(b)** cells treated with HBP-MPEG-*b*-PCL-FA nanoparticles for 10 min, 30 min, 1 h and 4 h.

administration, Resources, Software, Supervision, Validation, Visualization, Writing – original draft, Writing – review & editing. Sherif Domingo Tietilu: Data curation, Formal analysis, Investigation, Visualization. Oğuz Yücel: Data curation, Formal analysis, Investigation, Visualization, Writing – original draft, Writing – review & editing. Tuğba Erol: Data curation, Formal analysis. Zeynep Püren Akgüner: Data curation, Formal analysis. Hakan Darıcı;: Data curation, Formal analysis, Investigation. Emine Alarcin: Investigation, Formal analysis, Writing – original draft, Writing – review & editing. Serkan Emik: Investigation, Formal analysis, Supervision, Writing – original draft, Writing – review & editing.

Funding

This work was supported by the Scientific and Technological Research Council of Turkey (TUBITAK) and Research Fund of Istanbul University-Cerrahpasa (Grant numbers 117Z732 and FYL-2020-34,534).

Declaration of competing interest

The authors declare that they have no known competing financial interests or personal relationships that could have appeared to influence the work reported in this paper.

Data availability

Data will be made available on request.

Appendix A. Supplementary data

Supplementary data to this article can be found online at https://doi.org/10.1016/j.jddst.2023.104195.

References

[1] J. Wu, The enhanced permeability and retention (Epr) effect: the significance of the concept and methods to enhance its application, J. Personalized Med. 11 (2021) 771.
[2] M.A. Subhan, S.S.K. Yalamarty, N. Filipczak, F. Parveen, V.P. Torchilin, Recent advances in tumor targeting via Epr effect for cancer treatment, J. Personalized Med. 11 (2021) 571.
[3] M. Kanapathipillai, A. Brock, D.E. Ingber, Nanoparticle targeting of anti-cancer drugs that alter intracellular signaling or influence the tumor microenvironment, Adv. Drug Deliv. Rev. 79 (2014) 107–118.
[4] N. Patankar, D. Waterhouse, Nano-particulate drug delivery systems for camptothecins, Cancer Ther. 8 (2010) 90–104.
[5] V. Gyanani, J.C. Haley, R. Goswami, Challenges of current anticancer treatment approaches with focus on liposomal drug delivery systems, Pharmaceuticals 14 (2021) 835.
[6] S. Li, S. Xu, X. Liang, Y. Xue, J. Mei, Y. Ma, Y. Liu, Y. Liu, Nanotechnology: breaking the current treatment limits of lung cancer, Adv Healthc Mater 10 (2021), 2100078.
[7] L. Feng, Q. Huang, Z. Huang, H. Li, X. Qi, Y. Wang, Z. Liu, X. Liu, L. Lu, Optimized animal model of cyclophosphamide-induced bone marrow suppression, Basic Clin. Pharmacol. Toxicol. 119 (2016) 428–435.
[8] N. Yadav, S. Parveen, M. Banerjee, Potential of nano-phytochemicals in cervical cancer therapy, Clin. Chim. Acta 505 (2020) 60–72.
[9] M.S. Zaman, N. Chauhan, M.M. Yallapu, R.K. Gara, D.M. Maher, S. Kumari, M. Sikander, S. Khan, N. Zafar, M. Jaggi, S.C. Chauhan, Curcumin nanoformulation for cervical cancer treatment, Sci. Rep. 6 (2016) 1–14.
[10] A. Chrastina, K.A. Massey, J.E. Schnitzer, Overcoming in vivo barriers to targeted nanodelivery, Wiley Interdiscip. Rev. Nanomed. Nanobiotechnol. 3 (2011) 421–437.
[11] Y. Chen, K. Cheng, Advances of biological-camouflaged nanoparticles delivery system, Nano Res. 13 (2020) 2617–2624.
[12] Z.J. Huo, S.J. Wang, Z.Q. Wang, W.S. Zuo, P. Liu, B. Pang, K. Liu, Novel nanosystem to enhance the antitumor activity of lapatinib in breast cancer treatment: therapeutic efficacy evaluation, Cancer Sci. 106 (2015) 1429–1437.
[13] T. Sun, Y.S. Zhang, B. Pang, D.C. Hyun, M. Yang, Y. Xia, Engineered nanoparticles for drug delivery in cancer therapy, Angew. Chem., Int. Ed. 53 (2014) 12320–12364.
[14] F.U. Din, W. Aman, I. Ullah, O.S. Qureshi, O. Mustapha, S. Shafique, A. Zeb, Effective use of nanocarriers as drug delivery systems for the treatment of selected tumors, Int. J. Nanomed. 12 (2017) 7291–7309.
[15] S. Senapati, A.K. Mahanta, S. Kumar, P. Maiti, Controlled drug delivery vehicles for cancer treatment and their performance, Signal Transduct. Targeted Ther. 3 (2018) 1–19.
[16] L.P. Balogh, Nanomedicine in Cancer. *Nanomedicine in Cancer* 8 (2017) 1–814.
[17] S. Feng, J. Lu, K. Wang, D. Di, Z. Shi, Q. Zhao, S. Wang, Advances in smart mesoporous carbon nanoplatforms for photothermal–Enhanced synergistic cancer therapy, Chem. Eng. J. (2022), 134886.
[18] K. Wang, J. Lu, J. Li, Y. Gao, Y. Mao, Q. Zhao, S. Wang, Current trends in smart mesoporous silica-based nanovehicles for photoactivated cancer therapy, J. Contr. Release 339 (2021) 445–472.
[19] A. Wicki, D. Witzigmann, V. Balasubramanian, J. Huwyler, Nanomedicine in cancer therapy: challenges, opportunities, and clinical applications, J. Contr. Release 200 (2015) 138–157.
[20] C. Gao, D. Yan, Hyperbranched polymers: from synthesis to applications, Prog. Polym. Sci. 29 (2004) 183–275.
[21] B. Bahrami, M. Mohammadnia-Afrouzi, P. Bakhshaei, Y. Yazdani, G. Ghalamfarsa, M. Yousefi, S. Sadreddini, F. Jadidi-Niaragh, M. Hojjat-Farsangi, Folate-conjugated nanoparticles as a potent therapeutic approach in targeted cancer therapy, Tumor Biol. 36 (2015) 5727–5742.
[22] X. Zhao, H. Li, R.J. Lee, Targeted drug delivery via folate receptors, Expet Opin. Drug Deliv. 5 (2008) 309–319.
[23] R.I. Pinhassi, Y.G. Assaraf, S. Farber, M. Stark, D. Ickowicz, S. Drori, A.J. Domb, Y. D. Livney, Arabinogalactan-folic acid-drug conjugate for targeted delivery and target-activated release of anticancer drugs to folate receptor-overexpressing cells, Biomacromolecules 11 (2010) 294–303.
[24] M.R. Thalji, A.A. Ibrahim, G.A.M. Ali, Cutting-edge development in dendritic polymeric materials for biomedical and energy applications, Eur. Polym. J. 160 (2021), 110770.
[25] T. Gurunathan, S. Mohanty, S.K. Nayak, Hyperbranched polymers for coating applications: a review, Polym. Plast. Technol. Eng. 55 (2016) 92–117.
[26] Y. Li, S. Wang, F.X. Song, L. Zhang, W. Yang, H.X. Wang, Q.L. Chen, A PH-sensitive drug delivery system based on folic acid-targeted HBP-modified mesoporous silica nanoparticles for cancer therapy, Colloids Surf. A Physicochem. Eng. Asp. 590 (2020), 124470.
[27] C.M. Paleos, D. Tsiourvas, Z. Sideratou, L.A. Tziveleka, Drug delivery using multifunctional dendrimers and hyperbranched polymers, Expet Opin. Drug Deliv. 7 (2010) 1387–1398.
[28] A. Kavand, N. Anton, T. Vandamme, C.A. Serra, D. Chan-Seng, Synthesis and functionalization of hyperbranched polymers for targeted drug delivery, J. Contr. Release 321 (2020) 285–311.
[29] A. Bal Öztürk, N. Oğuz, H. Tekarslan Şahin, S. Emik, E. Alarçin, Design of an amphiphilic hyperbranched core/shell-type polymeric nanocarrier platform for drug delivery, Turk. J. Chem. 44 (2020) 518–534.
[30] R. Zhang, M. Tang, A. Bowyer, R. Eisenthal, J. Hubble, A novel PH- and ionic-strength-sensitive carboxy methyl dextran hydrogel, Biomaterials 26 (2005) 4677–4683.
[31] H. Park, H. Tsutsumi, H. Mihara, Cell-selective intracellular drug delivery using Doxorubicin and α-helical peptides conjugated to gold nanoparticles, Biomaterials 35 (2014) 3480–3487.

[32] M.G.Sokrates Tammer, Infrared and Raman Characteristic Group Frequencies: Tables and Charts, vol. 283, John Wiley & Sons, 2004.
[33] C.V. Rohatgi, N.K. Dutta, N.R. Choudhury, Separator membrane from crosslinked poly(vinyl alcohol) and poly(methyl vinyl ether-alt-maleic anhydride), Nanomaterials 5 (2015) 398–414.
[34] Y.B. Lim, S.M. Kim, Y. Lee, W.K. Lee, T.G. Yang, M.J. Lee, H. Suh, J.S. Park, Cationic hyperbranched poly(amino ester): a novel class of DNA condensing molecule with cationic surface, biodegradable three-dimensional structure, and tertiary amine groups in the interior, J. Am. Chem. Soc. 123 (2001) 2460–2461.
[35] M. Gou, X. Zheng, K. Men, J. Zhang, B. Wang, L. Lv, X. Wang, Y. Zhao, F. Luo, L. Chen, X. Zhao, Y. Wei, Z. Qian, Self-assembled hydrophobic honokiol loaded MPEG-PCL diblock copolymer micelles, Pharm. Res. (N. Y.) 26 (2009) 2164–2173.
[36] X. Shuai, T. Merdan, F. Unger, M. Wittmar, T. Kissel, Novel biodegradable ternary copolymers hy-PEI-g-PCL-b-PEG: synthesis, characterization, and potential as efficient nonviral gene delivery vectors, Macromolecules 36 (2003) 5751–5759.
[37] Y.-H. Hsieh, M.-F. Hsieh, C.-H. Fang, C.-P. Jiang, B. Lin, H.-M. Lee, Osteochondral regeneration induced by TGF-β loaded photo cross-linked hyaluronic acid hydrogel infiltrated in fused deposition-manufactured composite scaffold of hydroxyapatite and poly (ethylene glycol)-block-poly(ε-caprolactone), Polymers 9 (2017) 182.
[38] M. Guo, C. Que, C. Wang, X. Liu, H. Yan, K. Liu, Multifunctional superparamagnetic nanocarriers with folate-mediated and PH-responsive targeting properties for anticancer drug delivery, Biomaterials 32 (2011) 185–194.
[39] S.J. Lee, Y.H. Shim, J.S. Oh, Y. Il Jeong, I.K. Park, H.C. Lee, Folic-acid-conjugated pullulan/poly(DL-lactide-Co-glycolide) graft copolymer nanoparticles for folate-receptor-mediated drug delivery, Nanoscale Res. Lett. 10 (2015) 1–11.
[40] K.L. Nair, S. Jagadeeshan, , Nair S, A., G.S.V. Kumar, Folic acid conjugated δ-valerolactone-poly(ethylene glycol) based triblock copolymer as a promising carrier for targeted Doxorubicin delivery, PLoS One 8 (2013), e70697.
[41] D.H. Nguyen, J.W. Bae, J.H. Choi, J.S. Lee, K.D. Park, Bioreducible cross-linked pluronic micelles: PH-triggered release of Doxorubicin and folate-mediated cellular uptake, J. Bioact. Compat Polym. 28 (2013) 341–354.
[42] Y. Peng, J. Huang, H. Xiao, T. Wu, X. Shuai, Codelivery of temozolomide and SiRNA with polymeric nanocarrier for effective glioma treatment, Int. J. Nanomed. 13 (2018) 3467–3480.
[43] R. Singh, P. Kesharwani, N.K. Mehra, S. Singh, S. Banerjee, N.K. Jain, Development and characterization of folate anchored saquinavir entrapped PLGA nanoparticles for anti-tumor activity, Drug Dev. Ind. Pharm. 41 (2015) 1888–1901.
[44] S.W. Tsai, J.W. Liaw, F.Y. Hsu, Y.Y. Chen, M.J. Lyu, M.H. Yeh, Surface-modified gold nanoparticles with folic acid as optical probes for cellular imaging, Sensors 8 (2008) 6660–6673.
[45] K. Watanabe, M. Kaneko, Y. Maitani, Functional coating of liposomes using a folate-polymer conjugate to target folate receptors, Int. J. Nanomed. 7 (2012) 3679–3688.
[46] Y. Yang, Y. Zhao, J. Lan, Y. Kang, T. Zhang, Y. Ding, X. Zhang, L. Lu, Reduction-sensitive CD44 receptor-targeted hyaluronic acid derivative micelles for Doxorubicin delivery, Int. J. Nanomed. 13 (2018) 4361–4378.
[47] L. Papaioannou, A. Angelopoulou, S. Hatziantoniou, M. Papadimitriou, P. Apostolou, I. Papasotiriou, K. Avgoustakis, Folic acid-functionalized gold nanorods for controlled paclitaxel delivery: in vitro evaluation and cell studies, AAPS PharmSciTech 20 (2019) 1–13.
[48] O. Yücel, A. Şengelen, S. Emik, E. Önay-Uçar, N. Arda, G. Gürdağ, Folic acid-modified methotrexate-conjugated gold nanoparticles as nano-sized trojans for drug delivery to folate receptor-positive cancer cells, Nanotechnology 31 (2020), 355101.
[49] G. Hao, Z.P. Xu, L. Li, Manipulating Extracellular tumour PH: an effective target for cancer therapy, RSC Adv. 8 (2018) 22182–22192.
[50] Y. Wu, F. Jiao, S. Han, T. Fan, Y. Liu, W. Li, L. Hu, Y. Zhao, C. Chen, Construction of amphiphilic copolymer nanoparticles based on hyperbranched poly (Amine-Ester) and 1,2-dipalmitoyl-Sn-Glycero-3-Phosphoethanolamine as drug carriers for cancer therapy, Nanomedicine 7 (2011) 945–954.
[51] D.T. Birnbaum, J.D. Kosmala, D.B. Henthorn, L. Brannon-Peppas, Controlled release of β-Estradiol from PLAGA microparticles: the effect of organic phase solvent on encapsulation and release, J. Contr. Release 65 (2000) 375–387.
[52] E.H. Ahmed, A.E. Abdelhamid, M.E. Vylegzhanina, A.Y. Volkov, T.E. Sukhanova, M.M.H. Ayoub, Morphological and spectroscopical characterization of hyperbranched polyamidoamine–zwitterionic chitosan-encapsulated 5-FU anticancer drug, Polym. Bull. 1–19 (2020).
[53] E.S. Lee, K. Na, Y.H. Bae, Polymeric micelle for tumor PH and folate-mediated targeting, J. Contr. Release 91 (2003) 103–113.
[54] T.S. Anirudhan, B.S. Bini, V. Manjusha, Glycyrrhetinic acid conjugated zein capped aminated mesoporous silica nanoparticle-based dual drug delivery system for liver: a PH-dependent triggered release, J. Mol. Liq. 340 (2021), 116852.
[55] Z. Shariatinia, N. Pourzadi, Designing novel anticancer drug release vehicles based on mesoporous functionalized MCM-41 nanoparticles, J. Mol. Struct. 1242 (2021), 130754.
[56] Y. Liu, J. Liang, S. Wei, L. Liu, M. Liao, Nanoparticles based on β-conglycinin and chitosan: self-assembly, characterization, and drug delivery, J. Appl. Polym. Sci. 132 (2015).
[57] M. Zhou, X. Zhang, J. Xie, R. Qi, H. Lu, S. Leporatti, J. Chen, Y. Hu, Ph-sensitive poly(β-amino Ester)s nanocarriers facilitate the inhibition of drug resistance in breast cancer cells, Nanomaterials 8 (2018).
[58] W. Li, J. Sun, X. Zhang, L. Jia, M. Qiao, X. Zhao, H. Hu, D. Chen, Y. Wang, Synthesis and characterization of PH-responsive PEG-poly(β-amino ester) block copolymer micelles as drug carriers to eliminate cancer stem cells, Pharmaceutics (2020) 12.
[59] H. Wang, F. Xu, Y. Wang, X. Liu, Q. Jin, J. Ji, PH-responsive and biodegradable polymeric micelles based on poly(β-amino ester)-graft-phosphorylcholine for Doxorubicin delivery, Polym. Chem. 4 (2013) 3012–3019.
[60] (a) X. Zhang, L. Meng, Q. Lu, Z. Fei, P.J. Dyson, Targeted delivery and controlled release of Doxorubicin to cancer cells using modified single wall carbon nanotubes, Biomaterials 30 (2009) 6041–6047;
(b) W. Lei, C. Sun, T. Jiang, Y. Gao, Y. Yang, Q. Zhao, S. Wang, Polydopamine-coated mesoporous silica nanoparticles for multi-responsive drug delivery and combined chemo-photothermal therapy, Mater. Sci. Eng. C 105 (2019), 110103.
[61] H. Al Rashid, Preparation and characterization of PLGA loaded nanoparticles obtained from D. melanoxylon Roxb. leaves for their antiproliferative and antidiabetic activity, Int. J. Green Pharm. 11 (3) (2017).
[62] M.M. Joseph, S.R. Aravind, S.M.S. Varghese, T.T. Sreelekha, PST-Gold nanoparticle as an effective anticancer agent with immunomodulatory properties, Colloids Surf. B Biointerfaces 104 (2013) 32–39.
[63] A. Rastegar, S. Nazari, A. Allahabadi, F. Falanji, F.A.D.A. Dourbash, Z. Rezai, G. Majidi, Antibacterial activity of amino-and amido-terminated poly (amidoamine)-G6 dendrimer on isolated bacteria from clinical specimens and standard strains, Med. J. Islam. Repub. Iran 31 (2017) 64.
[64] D. Cosco, D. Paolino, R. Muzzalupo, C. Celia, R. Citraro, D. Caponio, M. Fresta, Novel PEG-coated niosomes based on bola-surfactant as drug carriers for 5-fluorouracil, Biomed. Microdevices 11 (5) (2009) 1115–1125.
[65] A. Jain, S.K. Jain, In vitro and cell uptake studies for targeting of ligand anchored nanoparticles for colon tumors, Eur. J. Pharmaceut. Sci. 35 (5) (2008) 404–416.
[66] M.E. Mathew, J.C. Mohan, K. Manzoor, S.V. Nair, H. Tamura, R. Jayakumar, Folate conjugated carboxymethyl chitosan–manganese doped zinc sulphide nanoparticles for targeted drug delivery and imaging of cancer cells, Carbohydr. Polym. 80 (2) (2010) 442–448.
[67] X. Zhang, L. Meng, Q. Lu, Z. Fei, P.J. Dyson, Targeted delivery and controlled release of Doxorubicin to cancer cells using modified single wall carbon nanotubes, Biomaterials 30 (2009) 6041–6047.